

# Understanding long-term carbon cycle trends: The late Paleocene through the early Eocene

N. Komar,<sup>1</sup> R. E. Zeebe,<sup>1</sup> and G. R. Dickens<sup>2,3</sup>

Received 13 June 2013; revised 5 September 2013; accepted 12 September 2013.

[1] The late Paleocene to the early Eocene (~58–52 Ma) was marked by significant changes in global climate and carbon cycling. The evidence for these changes includes stable isotope records that reveal prominent decreases in  $\delta^{18}\text{O}$  and  $\delta^{13}\text{C}$ , suggesting a rise in Earth's surface temperature ( $\sim 4^\circ\text{C}$ ) and a drop in net carbon output from the ocean and atmosphere. Concurrently, deep-sea carbonate records at several sites indicate a deepening of the calcite compensation depth (CCD). Here we investigate possible causes (e.g., increased volcanic degassing or decreased net organic burial) for these observations, but from a new perspective. The basic model employed is a modified version of GEOCARB III. However, we have coupled this well-known geochemical model to LOSCAR (Long-term Ocean-atmosphere Sediment Carbon cycle Reservoir model), which enables simulation of seawater carbonate chemistry, the CCD, and ocean  $\delta^{13}\text{C}$ . We have also added a capacitor, in this case represented by gas hydrates, that can store and release  $^{13}\text{C}$ -depleted carbon to and from the shallow geosphere over millions of years. We further consider accurate input data (e.g.,  $\delta^{13}\text{C}$  of carbonate) on a currently accepted timescale that spans an interval much longer than the perturbation. Several different scenarios are investigated with the goal of consistency amongst inferred changes in temperature, the CCD, and surface ocean and deep ocean  $\delta^{13}\text{C}$ . The results strongly suggest that a decrease in net organic carbon burial drove carbon cycle changes during the late Paleocene and early Eocene, although an increase in volcanic activity might have contributed. Importantly, a drop in net organic carbon burial may represent increased oxidation of previously deposited organic carbon, such as stored in peat or gas hydrates. The model successfully recreates trends in Earth surface warming, as inferred from  $\delta^{18}\text{O}$  records, the CCD, and  $\delta^{13}\text{C}$ . At the moment, however, our coupled modeling effort cannot reproduce the magnitude of change in all these records collectively. Similar problems have arisen in simulations of short-term hyperthermal events during the early Paleogene (Paleocene-Eocene Thermal Maximum), suggesting one or more basic issues with data interpretation or geochemical modeling remain.

**Citation:** Komar, N., R. E. Zeebe, and G. R. Dickens (2013), Understanding long-term carbon cycle trends: The late Paleocene through the early Eocene, *Paleoceanography*, 28, doi:10.1002/palo.20060.

## 1. Introduction

[2] Prominent decreases in the  $\delta^{18}\text{O}$  and  $\delta^{13}\text{C}$  of marine carbonate occurred over the late Paleocene and early Eocene

(LPEE; Figure 1) [Shackleton, 1986; Zachos *et al.*, 2001; Cramer *et al.*, 2009; Zachos *et al.*, 2010]. The drop in  $\delta^{18}\text{O}$  indicates a long-term warming trend, whereby Earth's surface at high latitudes and the deep ocean warmed by  $\sim 4^\circ\text{C}$  [Zachos *et al.*, 2001; Bijl *et al.*, 2009; Westerhold *et al.*, 2011; Hollis *et al.*, 2012]. Almost concurrently, planktic and benthic stable carbon isotope ratios gradually dropped by about 2‰, while deep-sea carbonate records at several sites indicate a deepening of the calcite compensation depth (CCD) [Hancock *et al.*, 2007; Leon-Rodriguez and Dickens, 2010]. The precise magnitude of CCD deepening is uncertain but was probably several hundred meters. Absolute ages surrounding the LPEE also remain uncertain; throughout this work, we assume the “Option-1” time scale presented by Westerhold *et al.* [2008] is close to being correct, such that the LPEE  $\delta^{13}\text{C}$  drop occurred from  $\sim 58.0$  to 52.5 Ma (Figure 1).

Additional supporting information may be found in the online version of this article.

<sup>1</sup>Department of Oceanography, University of Hawaii, Honolulu, Hawaii, USA.

<sup>2</sup>Department of Earth Sciences, Rice University, Houston, Texas, USA.

<sup>3</sup>Department of Geological Sciences, Stockholm University, Stockholm, Sweden.

Corresponding author: N. Komar, School of Ocean and Earth Science and Technology, University of Hawaii at Manoa, 1000 Pope Rd., MSB 507, Honolulu, HI 96822, USA. (komar@hawaii.edu)

©2013. American Geophysical Union. All Rights Reserved.  
0883-8305/13/10.1002/palo.20060

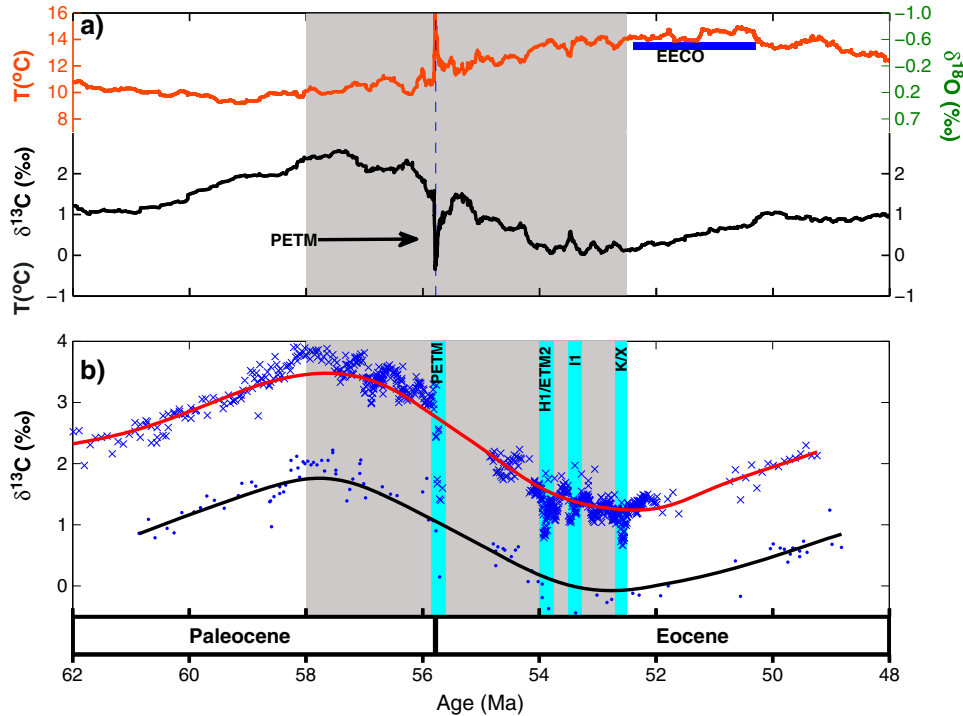


**Figure 1.** (a) Global benthic  $\delta^{18}\text{O}$  (orange) and  $\delta^{13}\text{C}$  (black) foraminiferal compilation based on data from *Cramer et al.* [2009]. Data shown here were smoothed using 10-point running average. Temperature estimates assume an ice-free world. The gray box approximately delineates the LPEE, and the horizontal dark blue line marks the Early Eocene Climatic Optimum (EECO), a time interval when temperature appears to have been warm, despite a rise in  $\delta^{13}\text{C}$ ; (b) Pacific and Atlantic Ocean  $\delta^{13}\text{C}$  (Sites 577 and 527) bulk sediment data (blue crosses) and benthic foraminifera (blue dots) with revised stratigraphy and refined age datums [*Dickens and Backman, 2013*]. The solid lines are smoothed regression curves using a local linear kernel estimator with a constant bandwidth of 1 Ma. Smoothed bulk sediment data are used to drive GEOCARB. Turquoise-shaded areas represent hyperthermals.

[3] This interval of the Cenozoic is also characterized by a series of short-lived hyperthermals, or transient episodes of warming. The Paleocene-Eocene Thermal Maximum (PETM), which occurred around 55.5 Ma, was the most prominent hyperthermal; however, at least two additional and significant warming events followed (ETM-2 or H-1 circa 53.7 Ma and K/X circa 52.5 Ma; Figure 1b) [*Lourens et al., 2005; Nicolo et al., 2007; Stap et al., 2009; Zachos et al., 2010; Leon-Rodriguez and Dickens, 2010*]. Each of the hyperthermals exhibits a negative carbon isotope excursion as well as a carbonate dissolution horizon in deep-sea sediments (above references). These events have been associated with rapid ( $< \sim 10^4$  years) and massive inputs of  $^{13}\text{C}$ -depleted carbon to the ocean-atmosphere system [*Dickens et al., 1997; above references; McInerney and Wing, 2011*]. For the PETM, several thousand petagrams of carbon ( $1 \text{ Pg} = 10^{15} \text{ g}$ ) represents a minimum estimate.

[4] The present study uses a combination of data analysis and numerical modeling to constrain the cause of several trends in records spanning the LPEE—in a broad sense, the large changes in background conditions surrounding the hyperthermals. These include the prominent drops in the  $\delta^{13}\text{C}$  of surface and deep ocean, the temperature rise, and the deepening of the CCD. Such modeling should

allow better understanding of long-term carbon cycling and possible relationships with the superimposed, transient hyperthermals.

[5] We assess the problem from two different perspectives. First, we focus on two mechanisms within the context of conventional views for the global carbon cycle (Figure 2). We examine whether an increase in volcanic degassing or, alternatively, a decrease in the net burial of organic carbon might have caused the long-term carbon cycle and climatic variations during the LPEE. Note that, from a modeling perspective, we cannot distinguish between decreased burial of organic carbon, increased oxidation of organic carbon, or some combination of both. We therefore refer to the sum of these processes as “net organic carbon burial” throughout this work. Second, we examine a mechanism that lies outside of conventional views for the global carbon cycle. Specifically, we added a dynamic capacitor that can store and release very large quantities of  $^{13}\text{C}$ -depleted carbon in the shallow geosphere over time. For this study, we focused on a gas hydrate capacitor, because this possibility has been suggested [*Dickens, 2003, 2011*]. In order to quantify the effects of these mechanisms, we first performed simple mass and isotope balance calculations and followed these by a more sophisticated analysis employing numerical modeling.

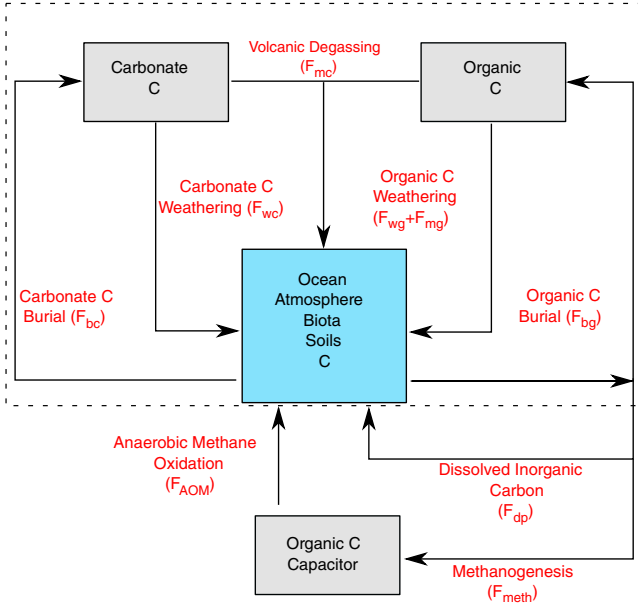


**Figure 2.** A box model of the long-term carbon cycle. Each box represents a reservoir, and arrows represent fluxes of carbon between the reservoirs. Dashed frame includes the standard carbon cycle [e.g. *Berner*, 1999], whereas the fluxes and reservoir outside of the frame illustrate a hypothetical organic capacitor (e.g. methane hydrates).  $F_{dp}$  - bicarbonate flux,  $F_{meth}$  - methanogenesis,  $F_{aom}$  - anaerobic oxidation of methane [*Dickens*, 2011]. For flux and mass values refer to Table 1.

## 2. Model Description

### 2.1. Basic Modules

[6] The overall modeling in this study couples two geochemical models: LOSCAR (Long-Term Ocean-Atmosphere Sediment Carbon Cycle Reservoir model) and a modified version of GEOCARB III. Both models are thoroughly documented [*Berner and Kothavala*, 2001; *Zeebe*, 2012] but we note key aspects here.

[7] LOSCAR includes the distribution of various biogeochemical tracers, such as total carbon ( $\text{TCO}_2$ ), total alkalinity (TA), dissolved phosphate ( $\text{PO}_4$ ), dissolved oxygen ( $\text{O}_2$ ), and stable carbon isotopes ( $\delta^{13}\text{C}$ ) of surface, intermediate and deep water and bulk sediments. Parameters such as  $[\text{CO}_2]$ ,  $[\text{CO}_3^{2-}]$ , pH, and calcite saturation state are then computed from predicted  $\text{TCO}_2$  and TA using chemistry routines explained by *Zeebe and Wolf-Gladrow* [2001]. In our simulations we used  $[\text{Ca}^{2+}] = 20 \text{ mmol kg}^{-1}$  and  $[\text{Mg}^{2+}] = 30 \text{ mmol kg}^{-1}$  as inferred from fluid inclusions in marine halites [*Lowenstein et al.*, 2001; *Horita et al.*, 2002], rather than the modern values of  $[\text{Ca}^{2+}] = 10 \text{ mmol kg}^{-1}$  and  $[\text{Mg}^{2+}] = 53 \text{ mmol kg}^{-1}$  [*Tyrrell and Zeebe*, 2004]. Warmer surface and bottom water temperatures in the late Paleocene and early Eocene have an impact on solubility and equilibrium constants. Bottom water temperatures are prescribed at  $8^\circ\text{C}$  for the late Paleocene (circa 58 Ma) and the model accounts for the effects of evolving temperature. Specifically, temperature changes as a function of  $\text{CO}_2$ , and this impacts equilibrium constants for reactions involving

dissolved  $[\text{Ca}^{2+}]$  and  $[\text{Mg}^{2+}]$ . The model also uses ocean basin volumes based on a Paleocene/Eocene topography by *Bice and Marotzke* [2002]. LOSCAR’s architecture, main components, and variables as well as process parameterization are described in detail by *Zeebe* [2012].

[8] GEOCARB III is a model developed by *Berner and Kothavala* [2001] to explain long-term variations in the exogenic carbon cycle. More specifically, it considers carbon exchange processes between geologic (crustal rocks and deeply buried sediments) and surficial (atmosphere and oceans) reservoirs (equation (1)). The balance of carbon fluxes between different reservoirs ultimately determines the atmospheric  $\text{CO}_2$  concentration [*Ridgwell and Zeebe*, 2005]. The two fundamental steady state equations embedded in GEOCARB III are

$$F_{wc} + F_{mc} + F_{wg} + F_{mg} = F_{bc} + F_{bg} \quad (1)$$

$$\delta_c F_{wc} + \delta_{mc} F_{mc} + \delta_g (F_{wg} + F_{mg}) = \delta_{bc} F_{bc} + (\delta_{bc} - \epsilon_g) F_{bg} \quad (2)$$

where parameters are described in Table 1. These two equations, or their time-dependent form, also lie at the core of other geochemical models [e.g., *Kump and Arthur*, 1999].

[9] The model assumes that during each 1 Myr period (the time step of GEOCARB III), the rate of burial of carbon as carbonates in sediments ( $F_{bc}$ ) is equal to the rate of weathering of carbon from silicates ( $F_{wsi}$ ) and carbonates ( $F_{wc}$ ). Therefore,  $F_{wsi} = F_{bc} - F_{wc}$ . This assumption is approximately true on a million year timescale because carbon in the ocean-atmosphere system has a relatively rapid turnover, which is a result of its very small carbon storage capacity compared to fluxes from and to the geologic reservoir. A more detailed explanation of the GEOCARB III model parameterization, its architecture, and processes can be found in *Berner and Kothavala* [2001].

[10] It is important to recognize that input data used in GEOCARB III modeling have a linearly interpolated  $\geq 10$  Myr resolution. Hence, the original GEOCARB III model cannot be used directly for investigating carbon cycling during the LPEE, because the input data are too coarse. Knowing the average values of bulk sediment  $\delta^{13}\text{C}$  ( $\delta_{bc}$ ) between 58 Ma and 52 Ma is critical because sediment burial rates of carbonate and organic carbon are calculated using the carbon isotopic data of ancient seawater. Therefore, it was necessary to modify GEOCARB III in order to capture the processes of the long-term carbon cycle during the LPEE more realistically. This modified version is referred to as the GEOCARB module.

[11] Unlike GEOCARB III, which implements a smoothed fit to  $\delta^{13}\text{C}$  data presented by *Veizer et al.* [1999] (over 10 million years time intervals), the GEOCARB module uses a much higher temporal resolution of the  $\delta^{13}\text{C}$ . We use  $\delta^{13}\text{C}$  records at Deep Sea Drilling Project (DSDP) Sites 527 and 577 (Figure 1b), which recently have been placed onto a common and current timescale [*Dickens and Backman*, 2013]. For the purposes of this study, the data were smoothed using a local linear kernel estimator with a constant bandwidth of 1 Ma (Figure 1b, solid lines). For more information on the statistical technique used here, see *Samworth and Poore* [2005] and *Poore et al.* [2006]. This approach eliminates aberrant model variations (caused by rapid fluctuations in the  $\delta^{13}\text{C}$  associated with the PETM and other hyperthermal events), while still capturing the

**Table 1.** Modeling Parameters<sup>a</sup>

Parameter:	Description	Initial Value Mass Balance	Initial Value Sim 2 (58 Ma)	Initial Value Sim 3 (62 Ma)
c, g	These subscripts refer to carbonate and organic carbon, respectively.			
$F_{wc}, F_{wg}$	Rate of release of carbon to the ocean-atmosphere-biosphere system via the weathering.	$F_{wc} = 16.0$ $F_{wg} = 10.0$	$F_{wc} = 16.37$ $F_{wg} = 3.13$	$F_{wc} = 18.76$ $F_{wg} = 3.13$
$F_{mc}, F_{mg}$	Rate of release of carbon to the ocean-atmosphere-biosphere system via the metamorphic/volcanic breakdown.	$F_{mc} = 6.0$	$F_{mc} = 6.04$ $F_{mg} = 1.89$	$F_{mc} = 5.89$ $F_{mg} = 1.86$
$F_{bc}, F_{bg}$	Burial rate of carbon.	$F_{bc} = F_{ws} + F_{wc}$ $F_{bg} = 10.0$	$F_{bc} = 21.12$ $F_{bg} = 6.31$	$F_{bc} = 24.3$ $F_{bg} = 5.34$
$F_{ws}$	Rate of uptake of atmospheric CO <sub>2</sub> via the weathering of Ca and Mg silicates followed by precipitation of the Ca and Mg as carbonates.	$F_{ws} = F_{mc}$	$F_{ws} = 4.75$	$F_{ws} = 5.55$
$F_{meth}, \delta_{meth}$	Methanogenesis and its isotopic value.			$F_{meth} = 1.0$ $\delta_{meth} = -70.0$
$F_{dp}, \delta_{dp}$	Bicarbonate flux and its isotopic value.			$F_{dp} = 1.0$ $\delta_{dp} = 10.0$
$F_{AOM}, \delta_{AOM}$	Anaerobic oxidation of methane and its isotopic value.			$F_{AOM} = 1.0$ $\delta_{AOM} = -70.0$
$M_{CAP}$	Mass of the capacitor.			3000 Pg C,
$M_{oc+atm}$	Mass of ocean + atmosphere.	irrelevant	27,139 Pg C	34,290 Pg C
$\delta$	$\delta^{13}C$ value (‰); $\delta_c$ average value for all carbonates, $\delta_g$ average value for all organic matter, $\delta_{mc}$ volcanic degassing, and $\delta_{bc}$ value for bulk sediment carbonates at time t, Figure 1b.	$\delta_c = 2.0$ $\delta_g = -21.2$ $\delta_{mc} = -4.0$ $\delta_{bc} = \text{calculated}$	$\delta_c = 2.0$ $\delta_g = -21.2$ $\delta_{mc} = -4.0$ $\delta_{bc} = 3.54$	$\delta_c = 2.0$ $\delta_g = -21.2$ $\delta_{mc} = -4.0$ $\delta_{bc} = 2.32$
$\epsilon_g$	Fractionation factor between organic carbon matter and carbonates.	$\epsilon_g = -31.0$	$\epsilon_g = -30.9$	$\epsilon_g = -30.1$
pCO <sub>2</sub>	Atmospheric carbon dioxide concentration (ppmv).	700.0	510.2	791.8

<sup>a</sup>Fluxes: 10<sup>12</sup> mol yr<sup>-1</sup>.

long-term trend of the  $\delta^{13}C$  over this time interval. This is justified by the fact that we are only investigating long-term carbon cycle behavior, rather than short-term fluctuations.

[12] Because the isotopic fractionation between organic carbon and carbonates ( $\epsilon_g$ ) is approximately equal to the difference between the  $\delta^{13}C$  of sedimentary carbonates ( $\delta_{bc}$ ) and  $\delta^{13}C$  of total organic carbon ( $\delta_{TOC}$ ) [Hayes *et al.*, 1999], the  $\epsilon_g$  also had to be recalculated:

$$\epsilon_g = \left[ \frac{\delta_{bc} + 1000}{\delta_{TOC} + 1000} - 1 \right] \times 10^3 \quad (3)$$

Values of  $\delta_{TOC}$  can be found for the late Paleocene [Erdman and Schorno, 1979; Macko and Pereira, 1990] and for the early Eocene [Erdman and Schorno, 1978a, 1978b, 1978c]. This adjustment leads to a decrease in  $\epsilon_g$  of about 1.0‰ between 58 Ma and 52 Ma (from  $\sim 31.0$ ‰ to  $\sim 30.0$ ‰). Interestingly, one might predict an increase in carbon isotope fractionation between dissolved inorganic carbon (DIC) and organic carbon during the LPEE due to rising pCO<sub>2</sub> [e.g., Freeman and Hayes, 1992]. The discrepancy may reflect a poor and incomplete record of  $\delta_{TOC}$  across this time interval. However, other than discontinuous records of organic  $\delta^{13}C$  from the central Arctic Ocean [Stein *et al.*, 2006; Sluijs and Dickens, 2012], an unusual location, the above references seemingly provide the only pertinent data available in the literature.

## 2.2. Coupling

[13] GEOCARB does not include ocean chemistry or sediments and hence cannot predict the position of the CCD

and its variation over time. In order to successfully reconcile and simulate the multimillion year trends observed during the late Paleocene and early Eocene, the computation of the CCD and its evolution throughout the studied time period is vital. Therefore, it was necessary to couple GEOCARB with the LOSCAR model (Figure 3). More precisely, the GEOCARB module has been implemented as a function that is called from within LOSCAR. Once LOSCAR is initiated, it uses the GEOCARB module to obtain the fluxes ( $F_{wc}$ ,  $F_{mc}$ ,  $F_{wg}$ ,  $F_{mg}$ ,  $F_{bg}$ , and  $F_{wsi}$ ) across the LPEE (58 to 52 Ma). LOSCAR then runs forward in time (starting at 58 Ma) calling the GEOCARB module at prescribed time increments. We set these increments to 1000 years and note that lower values will give smoother results. In turn, LOSCAR sends information to GEOCARB, such that fluxes are updated for LOSCAR every 1000 years. Using these fluxes and biogeochemical tracer distributions (TCO<sub>2</sub>, TA, PO<sub>4</sub>, O<sub>2</sub>,  $\delta^{13}C$ , and wt%CaCO<sub>3</sub> in sediments), different parameters were calculated, including atmospheric CO<sub>2</sub>, ocean pH, calcite and aragonite saturation state, and calcite compensation depth (see Figure 3).

## 3. Results and Discussion

### 3.1. Decoupled Mass Balance Experiments

[14] We first determined long-term responses of the ocean-atmosphere system to increased volcanic degassing and decreased net organic carbon burial using a “decoupled” mass balance approach (see supporting information). Examined responses were the evolution of  $\delta^{13}C$ , atmospheric

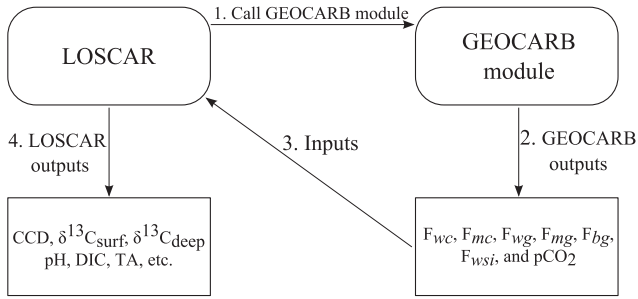


**Figure 3.** LOSCAR-GEOCARB coupling schematics (see text for description of variables).

$p\text{CO}_2$ , surface temperature, weathering fluxes, and the CCD (Figures S1 and S2). The primary purpose of these “experiments” (Table 2) was to examine the related effects, especially including the CCD, that result from changes in primary carbon fluxes to the exogenic carbon cycle over several millions of years (Figure 2).

[15] The basic results of these experiments are presented in a systematic manner (Figures S1 and S2) such that units shown on horizontal axes correspond to the factor by which the external carbon flux was increased or decreased. For example, 1.1 corresponds to an increase by 10%, and 0.9 corresponds to a decrease by 10%. To put such results into the context of the LPEE, the horizontal axes may be converted to the time domain. In particular, the horizontal axes can be viewed as representing the time interval between 58 and 52 Ma (going from left to right), over which volcanic degassing increased by 45% or organic carbon burial decreased by 25%.

[16] From a qualitative perspective, our results are common to those from similar modeling efforts. An increase in carbon fluxes from a  $^{13}\text{C}$ -depleted carbon source (e.g., the mantle) to the exogenic carbon cycle on the million year timescale should decrease the  $\delta^{13}\text{C}$  of the ocean and atmosphere (Figures S1a and S2a), increase atmospheric  $p\text{CO}_2$  and temperature (Figures S1b and S2b), enhance continental weathering (Figures S1c and S2c), and deepen the CCD (Figures S1d and S2d). The same is true for a decrease in carbon fluxes from the exogenic carbon cycle to a  $^{13}\text{C}$ -depleted carbon reservoir (e.g., organic carbon in sediments).

[17] We emphasize that model results depend on initial masses, fluxes and parameters (Table 1). This is obvious in generic model exercises [e.g., Berner *et al.*, 1983; Berner, 1990; Dickens, 2001a]. For example, both  $p\text{CO}_2$  curves, the one predicted by LOSCAR and the other one pre-

dicted by simple mass balance, are identical because both approaches are based on the same weathering parameterization (equations (S5) and (S6) and Figures S1b and S2b in the supporting information). The modeled overall temperature increase ( $\Delta T \approx 4^\circ\text{C}$ ) was calculated assuming an equilibrium Earth system sensitivity ( $\Delta T_{\times 2}$ ) equal to the canonical value of the fast-feedback sensitivity of  $3^\circ\text{C}$  [IPCC, 2007]. Carbonate and silicate weathering fluxes, displayed in Figures S1c and S2c, come directly from equations (S5) and (S6) in the supporting information. The position of the CCD, shown in Figures S1d and S2d, was computed with LOSCAR by allowing the model to reach steady state after a prescribed volcanic degassing or organic burial perturbation. The overall CCD deepening is around 1.5 km in both increased volcanic degassing scenario and decreased net organic carbon burial scenario.

[18] The model results are then compared to the available  $\delta^{13}\text{C}$  data, the paleotemperature record and the paleo-CCD trends. The global paleotemperature was inferred from the  $\delta^{18}\text{O}$  composition of benthic foraminifera (Figure 1a) by using the linear equation given by Shackleton [1974] and reviewed by Bemis *et al.* [1998]. According to the temperature reconstruction, the average deep ocean temperature of the late Paleocene was around  $10^\circ\text{C}$  and steadily increased to about  $14^\circ\text{C}$  in the early Eocene (Figure 1a). The early Paleogene CCD remains poorly constrained [Pälike *et al.*, 2012]. Nonetheless, there are several sites from across the Indian and Pacific Oceans that at present day lie at  $>4800$  m water depth and that contain early Eocene sediment lacking carbonate [Van Andel, 1975; Zhou and Kyte, 1992; Expedition 329 Scientists, 2011]. The CCD probably never dropped below 4500 m in the early Paleogene [Van Andel, 1975] and probably deepened less than 1000 m during the LPEE [Hancock *et al.*, 2007; Leon-Rodriguez and Dickens, 2010]. Despite known issues, the results are qualitatively consistent with observations. With available data, even the rudimentary “experiments” provide a reasonable first-order answer to carbon cycle changes across the LPEE.

[19] Evaluation of global carbon cycle perturbations from a true carbon mass balance perspective (i.e., including ocean carbon chemistry) provides a powerful means to discriminate between possible mechanisms. This is well known from papers discussing short-term events in geological time, including the early Paleogene hyperthermals [Dickens *et al.*, 1997; Zeebe *et al.*, 2009], but also holds over much longer time intervals. Given our two “experiments,” changes in volcanic degassing and organic carbon burial clearly impact global carbon cycle differently. Assuming constant carbon isotope composition of all fluxes as well as constant isotope

**Table 2.** Summary of All Experiments and Simulations Performed in This Study

	Explanation	Figure Number
A + N Experiment 1	Mass balance + LOSCAR CCD calculation: increased volcanic degassing scenario	Figure S1
A + N Experiment 2	Mass balance + LOSCAR CCD calculation: decreased organic burial scenario	Figure S2
Simulation 1	LOSCAR + GEOCARB module (standard parameters: $\text{ACT} = 0.09^\circ\text{C}^{-1}$ , $\Delta T_{\times 2} = 2.3^\circ\text{C}$ )	Figure 4
Simulation 2	LOSCAR + GEOCARB module ( $\text{ACT} = 0.05^\circ\text{C}^{-1}$ , $\Delta T_{\times 2} = 3^\circ\text{C}$ )	Figure 5
Simulations 3 and 4	LOSCAR, methane hydrate capacitor (Simulation 3, DIC:TA = 1:0, $\Delta T_{\times 2} = 3^\circ\text{C}$ ) (Simulation 4, DIC:TA = 1:1, $\Delta T_{\times 2} = 3^\circ\text{C}$ )	Figure 6

fractionation (see supporting information), the “per carbon mol” effects of volcanic degassing and net organic burial upon surface ocean  $\delta^{13}\text{C}$  and the CCD are substantially different (Figures S1 and S2 and Table S1). The difference is due to the fact that carbon emissions from volcanoes are much less depleted in  $^{13}\text{C}$  ( $\delta^{13}\text{C} \sim -4$  to  $-5\text{‰}$ ) than organic carbon buried in sediments ( $\delta^{13}\text{C} \sim -30\text{‰}$ ) [Lasaga *et al.*, 1985; Kump and Arthur, 1999]. Hence, an increase in carbon emissions from volcanoes (either from the mantle or metamorphism of upper crust) has a much smaller effect on ocean  $\delta^{13}\text{C}$  but a much greater impact on the CCD than a decrease in net burial of organic carbon. In other words, for the same  $\delta^{13}\text{C}$  excursion, the CCD change is much greater if the carbon originates from mantle. This is best illustrated by calculating the per mole effects of volcanic degassing and net organic carbon burial on the  $\delta^{13}\text{C}$  and the CCD (Table S1). To first order, if increased volcanic degassing was the sole cause for the observed drop in  $\delta^{13}\text{C}$  of the surface ocean during the LPEE, the CCD should have deepened three times ( $\frac{\Delta\delta^{13}\text{C}}{\Delta F_{bg}} > 3 \times \frac{\Delta\delta^{13}\text{C}}{\Delta F_v}$ ) as much as if decreased organic carbon burial was the sole cause.

[20] According to the results presented above, it is very unlikely that increased volcanic degassing was the main cause of carbon cycle changes during the LPEE, because this would have pushed the CCD far deeper than allowed by observations (Figure S1). However, excess volcanism might have contributed to overall climate change across the time interval. From a conventional view of the global carbon cycle, we agree with Kurtz *et al.* [2003]: A decrease in the net burial of organic carbon seems the most plausible explanation for the observed drop in  $\delta^{13}\text{C}$  from the late Paleocene through the early Eocene.

### 3.2. Coupled LOSCAR and GEOCARB Modeling

[21] We next simulated the evolution of the exogenic carbon cycle during the LPEE using the coupled GEOCARB-LOSCAR model (Simulation 1; Table 2). This simulation (Figure 4) uses new input data (e.g.,  $\delta_{bc}$  and  $\varepsilon_g$ ), but most GEOCARB parameters and variables were set to standard values described by Berner and Kothavala [2001]. GEOCARB predicts a 6% increase in volcanic degassing between 58 and 52 Ma, which partly governs the increase in  $p\text{CO}_2$  (Figure 4a). The outcome of the experiment (Figure 4) is predominantly a result of new input data ( $\delta_{bc}$  and  $\varepsilon_g$ , see above), which are the main drivers of the model. However, in reality, the  $\delta^{13}\text{C}$  of the surface ocean is set by carbon input and output fluxes, not the other way around.

[22] The trends are mainly driven by a decrease in net burial of organic carbon predicted by the GEOCARB module. The initial and final organic carbon burial fluxes are  $6.3 \times 10^{18}$  mol Myr $^{-1}$  at 58 Ma and  $\sim 4.4 \times 10^{18}$  mol Myr $^{-1}$  at 53 Ma, respectively. These values agree reasonably well with independent estimates made from the abundance of organic carbon in various types of sedimentary rocks [Berner and Canfield, 1989]. The results presented by Berner and Canfield [1989], just like GEOCARB III, have a 10 Myr temporal resolution. Despite this low resolution, they suggest organic burial rates around  $6.7 \times 10^{18}$  mol Myr $^{-1}$  at 60 Ma (the Cenozoic maxima), which then decrease slightly throughout the Cenozoic.

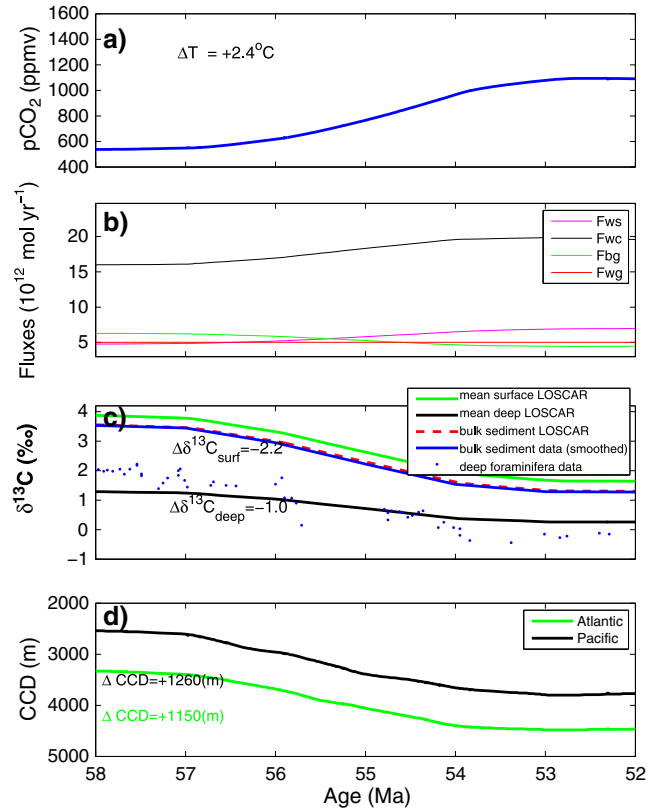


**Figure 4.** LOSCAR + GEOCARB module simulation results. The response of the ocean-atmosphere system due to changes of fluxes predicted by the GEOCARB module (new input data); (a)  $\text{CO}_2$ ; (b) silicate weathering ( $F_{ws}$ ), carbonate weathering ( $F_{wc}$ ), organic carbon burial ( $F_{bg}$ ), organic carbon weathering ( $F_{wg}$ ); (c)  $\delta^{13}\text{C}$  of both surface and deep ocean; and (d) calcite compensation depth. LA: low-latitude surface Atlantic, LP: low-latitude surface Pacific, DA: deep Atlantic.

[23] Other modeling studies [Kurtz *et al.*, 2003; Hilting *et al.*, 2008] have identified the latest Paleocene and early Eocene as a time interval marked by decreasing burial of organic carbon, although with approaches somewhat different from the ones implemented in this study. Between 57 and 52 Ma, Kurtz *et al.* [2003] and Hilting *et al.* [2008] suggested decreases in  $F_{bg}$  from  $\sim 5.8$  to  $\sim 4.1 \times 10^{18}$  mol Myr $^{-1}$  and from  $\sim 8.5$  to  $\sim 7.5 \times 10^{18}$  mol Myr $^{-1}$ , respectively. However, Kurtz *et al.* [2003] did not address the evolution of atmospheric  $p\text{CO}_2$ , carbonate chemistry of seawater, or the CCD. Basically, their carbon cycle consists of a single reservoir with one input (weathering) and two outputs (organic and carbonate carbon burial). While Hilting *et al.* [2008] included estimates for  $p\text{CO}_2$  and seawater chemistry, the CCD was omitted. Note also that some stable isotope records used in previous modeling exercises were on incorrect timescales, such that inflections in  $\delta^{13}\text{C}$  at some sites were offset by 0.5 Myr or more [Dickens and Backman, 2013].

[24] The decrease in net organic carbon burial calculated by the GEOCARB module does not necessarily imply decreased burial of organic carbon into marine or terrestrial sediments. From a standard carbon cycle perspective

(Figure 2), it could equally well represent an increase in the weathering of organic matter ( $F_{wg} + F_{mg}$ ). As discussed below, it could also represent a discharge from an organic carbon capacitor, such as increased methane input from the seafloor or increased oxidation of peat [Dickens, 2003; Kurtz *et al.*, 2003]. In all cases, a decrease in net organic carbon burial should result in higher  $\text{CO}_2$  and a greater mass of carbon in the combined ocean-atmosphere reservoir (Figure 4a, Simulation 1). However, there is a problem. Assuming that atmospheric  $\text{CO}_2$  was the main control on global temperature during the LPEE, and assuming a modest Earth system sensitivity ( $\Delta T_{\times 2}$  of  $2.3^\circ\text{C}$ , standard GEOCARB III value), this scenario cannot explain an  $\sim 4^\circ\text{C}$  warming across the LPEE, as might be inferred from benthic foraminifera  $\delta^{18}\text{O}$  values and other proxies. Instead, the calculated temperature rise is only around  $2.4^\circ\text{C}$ .

[25] Due to the predicted  $p\text{CO}_2$  and temperature rises, carbonate and silicate weathering fluxes accelerate across the LPEE. In turn, this increases the carbonate ion supply to the ocean and thus, the concentration of  $\text{CO}_3^{2-}$ . The position of the carbonate compensation depth (CCD) is ultimately controlled on long time frames by the requirement that riverine carbon input fluxes need to balance carbonate burial output fluxes. Hence, the enhanced weathering causes a deepening of the CCD from about 57 Ma to 52 Ma, as inferred from carbonate accumulation records at several locations [Hancock *et al.*, 2007; Leon-Rodriguez and Dickens, 2010]. Again, there is a problem. According to Simulation 1, the CCD deepens by 1260 m in the Pacific and 1150 m in the Atlantic during the LPEE (Figure 4d), which is probably larger than allowed from sediment records.

[26] Carbon fluxes in GEOCARB are calculated by supplying the model with the  $\delta^{13}\text{C}$  data of the bulk carbonate ( $\delta_{bc}$  in equation (2)). On the other hand, the  $\delta^{13}\text{C}$  of the bulk carbonate in LOSCAR is controlled by carbon inputs and outputs and their respective isotopic values, which are supplied by GEOCARB. In theory, this means that the  $\sim 2.0\text{‰}$  decrease of surface ocean  $\delta^{13}\text{C}$  between 58 and  $\sim 52$  Ma prescribed by GEOCARB should be the same in LOSCAR, which is the case. The  $\delta^{13}\text{C}$  of the surface ( $\delta^{13}\text{C}_{\text{surf}}$ ) in LOSCAR is then calculated using an offset from the bulk sediment stable isotope value of  $0.5\text{‰}$ . The offset was inferred based on the difference between bulk carbonate  $\delta^{13}\text{C}$  record and planktonic foraminifera  $\delta^{13}\text{C}$  during the LPEE [Shackleton *et al.*, 1984].

[27] Unlike surface ocean  $\delta^{13}\text{C}$ , which is independent of internal oceanic processes, at least on long timescales, deep ocean  $\delta^{13}\text{C}$  (and therefore the vertical gradient) is also controlled by the biological pump and vertical mixing [Kump, 1991]. The maximum value of the gradient primarily depends on the ratio of nutrients to DIC [Hilting *et al.*, 2008]. This implies that as long as the ratio of nutrients and DIC remains constant over time, so will the  $\delta^{13}\text{C}$  gradient between the surface and deep ocean. In LOSCAR, biological uptake is parameterized using phosphate concentrations, which are prescribed and constant over time in the present simulations. On the other hand, due to increased  $p\text{CO}_2$  and enhanced weathering between 58 and 52 Ma, DIC of the ocean increases. Therefore, the modeled phosphate/DIC ratio decreases through time, and the surface to deep  $\delta^{13}\text{C}$  gradient diminishes (Figure 4c). This result is consistent with one set of observations, namely the difference between

planktonic foraminifera  $\delta^{13}\text{C}$  and benthic foraminifera  $\delta^{13}\text{C}$ , which lessened by about  $1\text{‰}$  at multiple sites during the LPEE [Hilting *et al.*, 2008]. However, bulk sediment  $\delta^{13}\text{C}$  approximately paralleled benthic foraminifera  $\delta^{13}\text{C}$  during the LPEE (Figure 1b). Because bulk sediment comprises mostly calcareous nannofossils, which lived in surface water, this would suggest minimal change in the surface to deep  $\delta^{13}\text{C}$  gradient. Unlike the model employed by Hilting *et al.* [2008], the coupled GEOCARB-LOSCAR approach does not use the deep ocean  $\delta^{13}\text{C}$  record as input data, but rather predicts this curve. This allows a detailed examination of various mechanisms (e.g., biological pump, biological productivity, rain ratio, etc.) and their effect on the surface to deep gradient of  $\delta^{13}\text{C}$ , which might allow us to better constrain the model.

### 3.3. Earth System Sensitivity and Biological Pumping

[28] In the original version of GEOCARB III, Earth system sensitivity ( $\Delta T_{\times 2}$ ) was set at  $2.3^\circ\text{C}$  per doubling of atmospheric  $\text{CO}_2$  during ice-free periods. Recent studies suggest that the  $\Delta T_{\times 2}$  was probably  $3^\circ\text{C}$  or higher for much of the Cenozoic [Park and Royer, 2011]. Furthermore, the atmospheric  $p\text{CO}_2$  predicted by GEOCARB (in the original and in our model) strongly depends on a parameter referred to as ACT. This is a coefficient that expresses the effect of temperature upon the rate of mineral dissolution during weathering. Value for ACT used in GEOCARB III simulation ranges from  $0.06$  to  $0.12^\circ\text{C}^{-1}$ , based on the field study conducted by Brady *et al.* [1999]. However, on the basis of paleo- $\text{CO}_2$  information and model analysis, Park and Royer [2011] showed that  $\Delta T_{\times 2}$  correlates inversely with ACT. They suggested ACT values as low as  $0.03^\circ\text{C}^{-1}$ , which would be in the range of laboratory studies of volcanic glasses [Gislason and Oelkers, 2003] and field studies of basaltic river samples from Iceland [Gislason *et al.*, 2009]. A lower ACT value translates into a weaker weathering feedback, meaning that for an equal rise in atmospheric  $\text{CO}_2$ , a change in silicate fluxes would be smaller.

[29] Simulation 1 failed to reproduce the expected rises in atmospheric  $p\text{CO}_2$  and surface temperature. Thus, we performed an additional simulation with a new set of values for  $\Delta T_{\times 2}$  and ACT. Simulation 2 (Figure 5) assumes an Earth system sensitivity of  $3^\circ\text{C}$  per doubling of  $p\text{CO}_2$  and an ACT of  $0.05^\circ\text{C}^{-1}$ .

[30] The new model run shows that a higher Earth system sensitivity alone minimally affects calculated temperatures on the 6 Myr timescale. This result, perhaps nonintuitive, reflects the definition of Earth system sensitivity and the way weathering is incorporated into GEOCARB. A larger  $\Delta T_{\times 2}$  creates a stronger silicate weathering feedback, which dampens any  $p\text{CO}_2$  rise. In turn, lower  $p\text{CO}_2$  relates to lower temperature and weaker weathering. On the other hand, changes in the weathering parameter ACT greatly influence the predicted  $p\text{CO}_2$ . By using a low-end estimate for ACT, much larger rises in  $p\text{CO}_2$  and temperature occur. Indeed, the observed change between 58 and 52 Ma ( $4.0^\circ\text{C}$ ) is on par with observations (Figure 5a). However, there are two problems. First, the change in long-term temperature leads the change in  $\delta^{13}\text{C}$  by several hundreds of thousands of years (Figure 1a). Consequently, some component of the temperature rise was likely unrelated to the primary cause of the

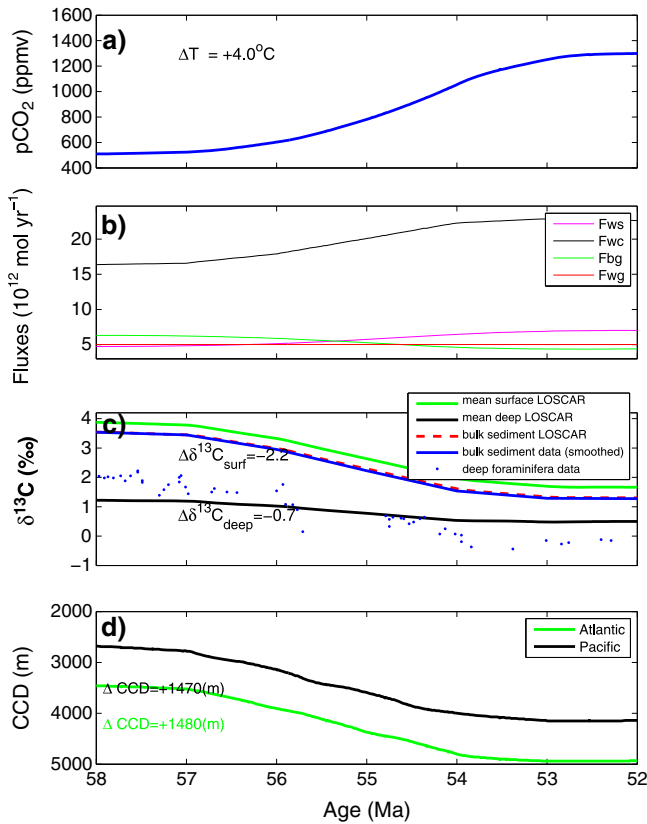


**Figure 5.** LOSCAR + GEOCARB module simulation results (new input data +  $ACT = 0.05^{\circ}\text{C}^{-1}$  and  $\Delta T_{\times 2} = 3^{\circ}\text{C}$ ).

carbon isotope excursion. Second, due to higher  $p\text{CO}_2$  and temperature, carbonate and silicate weathering fluxes are accelerated, so they exceed those predicted in Simulation 1. As a consequence, the deep ocean  $\Delta\delta^{13}\text{C}$  is smaller and the CCD deepening is more pronounced ( $\sim 1470$  and  $\sim 1480$  m in the Pacific and Atlantic Oceans, respectively) than in the previous simulation. In summary, while Simulation 2 produces warming consistent with certain views linking  $p\text{CO}_2$  and temperature, it conflicts with basic observations regarding the sedimentary record, including those pertaining to the global carbon cycle (deep ocean  $\delta^{13}\text{C}$  and the CCD).

[31] Assuming that the decrease in planktic to benthic foraminifera  $\delta^{13}\text{C}$  across the LPEE faithfully represents a past decrease in surface to deep water  $\delta^{13}\text{C}$ , a possible mechanism to reconcile the inferred temperature change would be through a decrease in the efficiency of the biological pump [Hilting *et al.*, 2008]. However, a weaker biological pump would lead to a deeper CCD, everything else being constant. This is due to the fact that a weaker biological pump decreases  $\text{CaCO}_3$  production and raises the  $\text{CaCO}_3$  saturation state of the ocean. Basically, the deep-sea carbonate ion concentration increases, so the CCD deepens, which instigates more precipitation to counteract the higher saturation state (i.e., a stabilizing feedback) [Zeebe and Westbroek, 2003]. Thus, if  $\text{CaCO}_3$  production dropped between 58 and 52 Ma, the simulated CCD becomes even more disparate from available CCD reconstructions for the time interval.

[32] Surface  $\delta^{13}\text{C}$  records used in previous modeling exercises [e.g., Hilting *et al.*, 2008] derive from anal-

yses of morozovellids and acariniids. These planktonic foraminifera genera almost assuredly hosted photosymbionts, and it has long been suspected that they do not record surface water  $\delta^{13}\text{C}$  [D'Hondt *et al.*, 1994; Birch *et al.*, 2012]. Instead, they seem enriched in  $^{13}\text{C}$  relative to surrounding water, typically by more than 1‰, but this depends on several factors. Notably, during warm time intervals, such as the PETM and the Middle Eocene Climatic Optimum, the  $\delta^{13}\text{C}$  of these genera decreases more than in other carbon-bearing phases of the ocean [McInerney and Wing, 2011; Edgar *et al.*, 2012].

[33] We have not fully considered the alternative: a stronger biological pump during the LPEE. This might produce a fairly consistent scenario with respect to changes in temperature,  $\Delta\text{CCD}$  and  $\Delta\delta^{13}\text{C}_{\text{deep}}$ . Accelerated weathering during the LPEE could lead to a higher supply of  $\text{PO}_4$  from land to ocean and a more constant  $\text{PO}_4/\text{DIC}$  ratio in the model. As a consequence, biological export during the LPEE would increase, the surface to deep ratio of  $\delta^{13}\text{C}$  would remain constant, and the CCD deepening would be less pronounced than in Simulation 2.

[34] Another factor that could offset CCD overdeepening (Simulation 2) is a concomitant rise in sea level, something that is not considered in our model. Early work suggested a major transgression during the LPEE, with an amplitude between 30 and 70 m [Haq *et al.*, 1987; Miller *et al.*, 1997]. This would result in greater burial of  $\text{CaCO}_3$  on the shelf and therefore less burial of  $\text{CaCO}_3$  in the open ocean because the input (riverine) and output (burial) fluxes of carbonate species have to balance [Zeebe and Westbroek, 2003]. There are, however, two problems with this mechanism. First, more recent compilations for sea level [Müller *et al.*, 2008] show no major sea level rise coincident with the LPEE. Second, a rise in sea level should lead to a higher organic carbon burial. With an increase in sea level, the area available for shallow water deposition increases, more organic matter can be buried faster, and organic matter has less time to be oxidized. This contradicts the predicted decrease in net organic carbon burial during the LPEE.

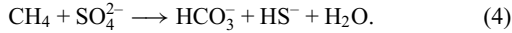
### 3.4. Inclusion of an Organic Capacitor and Release of Methane From the Seafloor as a Specific Example

[35] The above scenarios for the long-term carbon cycle changes are mostly “divorced” from the hyperthermals. That is, while they might be offered as potential explanations for the broad decrease in  $\delta^{13}\text{C}$  spanning the LPEE, they offer no insight to the well-known series of rapid and massive injections of  $^{13}\text{C}$ -depleted carbon that occurred within the time interval (Figure 1). Examination of the GEOCARB module (Figure 2) shows the reason: There is no means to store massive amounts of  $^{13}\text{C}$ -depleted carbon and return it to the ocean or atmosphere quickly.

[36] It is possible that the major long-term carbon cycle changes spanning the LPEE were unrelated to the short-term carbon cycle perturbations across the hyperthermals. Alternatively, one might recognize that the decrease in net organic carbon burial predicted by the model (Experiment 2, above) does not differentiate between diminished burial or greater oxidation, and it does not provide information on the location of modified organic carbon fluxes (e.g., shelf, slope, or land). The long-term and short-term carbon cycle changes

during the LPEE can be linked, at least from a modeling perspective, by adding a large and dynamic organic carbon capacitor to the exogenic carbon cycle [Berner, 1987; Dickens, 2003; Kurtz *et al.*, 2003]. Effectively, there would be some reservoir in the shallow geosphere that could store massive amounts of  $^{13}\text{C}$ -depleted carbon over time and release such carbon to the ocean and atmosphere at variable rates depending on environmental change. Suggested possibilities have included methane in marine sediment and peat on land [Dickens, 2003; Kurtz *et al.*, 2003].

[37] We next consider the LPEE as representing slow release of  $^{13}\text{C}$ -depleted carbon from a large, dynamic organic carbon capacitor and choose seafloor methane as a specific case. This requires two basic modifications to our modeling framework. First, the timescale of interest needs expansion. The drop in  $\delta^{13}\text{C}$  across the LPEE goes from the absolute high to the near low in carbon isotope records covering the entire Cenozoic. This suggests that at  $\sim 58$  Ma, the ocean-atmosphere system was far outside of multimillion year quasi steady state conditions. More specifically, 58 Ma would be a time when the organic capacitor had already stored large amounts of carbon. We therefore started the modeling at the point where  $\delta^{13}\text{C}$  is about average for the Cenozoic (62 Ma). Second, the GEOCARB model needs modification to include the additional box, which lies outside of the traditional exogenic reservoirs (Figure 2). Following Dickens [2003] and Dickens [2011], we connect gas hydrate systems to the ocean and atmosphere through some basic fluxes: (1) a small fraction of conventional organic carbon burial ( $F_{bg}$ ) goes through methanogenesis; (2) methanogenesis produces  $^{13}\text{C}$ -rich bicarbonate that returns to the ocean ( $F_{dp}$ ) and  $^{13}\text{C}$ -depleted methane that can remain in sediment ( $F_{meth}$ ); and (3) methane returns to the ocean through anaerobic oxidation of methane (AOM) and production of bicarbonate ( $F_{AOM}$ ). The latter reaction can be expressed as [Reeburgh, 1976]



Importantly, addition of such a capacitor changes the mathematical expressions (equations (1) and (2)), because they need to include the new fluxes:

$$F_{wc} + F_{mc} + F_{wg} + F_{mg} + F_{AOM} + F_{dp} = F_{bc} + F_{bg} + F_{dp} + F_{AOM} \quad (5)$$

$$\begin{aligned} \delta_c F_{wc} + \delta_{mc} F_{mc} + \delta_g (F_{wg} + F_{mg}) + \delta_{AOM} F_{AOM} + \delta_{dp} F_{dp} \\ = \delta_{bc} F_{bc} + (\delta_{bc} - \varepsilon_g) F_{bg} + \delta_{dp} F_{dp} + \delta_{AOM} F_{AOM} \end{aligned} \quad (6)$$

[38] The initial conditions at 62 Ma (e.g., masses, volcanic degassing flux, carbonate and silicate weathering rates, etc.) for these simulations were similar to those in the original GEOCARB module but with modifications to account for the small steady state inputs from the capacitor (Figure 1b). As a starting point, we use the quasi steady state fluxes suggested in previous work [Dickens, 2011]. Unlike in our previous simulations, however, most parameters in GEOCARB (e.g., organic carbon burial, isotope fractionation, and volcanic degassing) are assumed to be constant over time. This means, after 62 Ma ( $t > 0$ ), responses in the global carbon cycle become independent of the GEOCARB module; they are calculated by LOSCAR with the forcing achieved by changing the balance between inputs ( $F_{meth}$ ) and

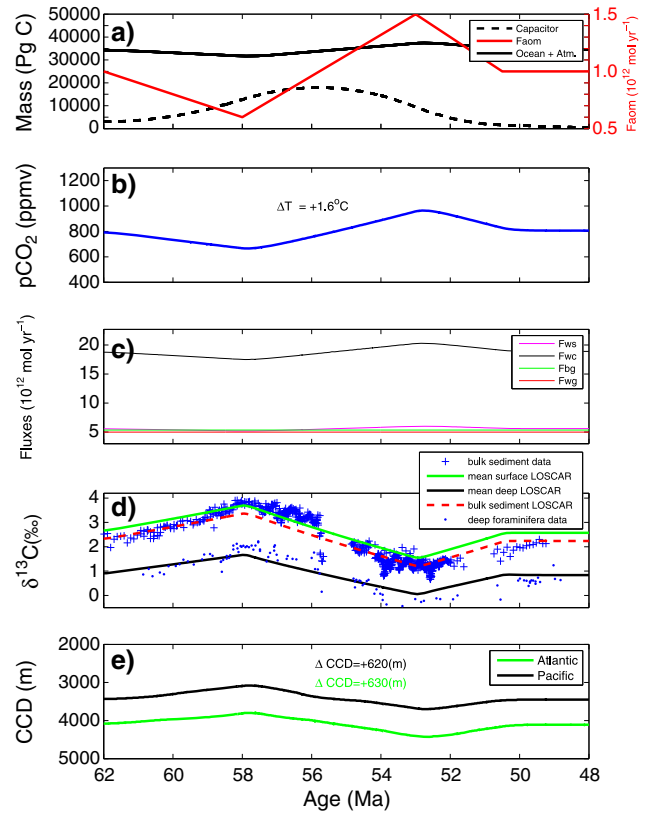


**Figure 6.** LOSCAR carbon capacitor simulation results. The response of the ocean-atmosphere system due to the prescribed  $F_{AOM}$  changes from the carbon capacitor; (a)  $F_{AOM}$  forcing and reservoirs' masses over time; (b)  $\text{CO}_2$ ; (c) silicate weathering ( $F_{ws}$ ), carbonate weathering ( $F_{wc}$ ), organic carbon burial ( $F_{bg}$ ), and organic carbon weathering ( $F_{wg}$ ); (d)  $\delta^{13}\text{C}$  of surface and deep ocean and bulk sediment; and (e) calcite compensation depth. LA: low Atlantic, LP: low Pacific, DA: deep Atlantic. No alkalinity contribution from AOM (DIC:TA = 1:0).

outputs ( $F_{AOM}$ ) to the gas hydrate capacitor. Crucially, surface ocean  $\delta^{13}\text{C}$  is now predicted rather than prescribed, and the ocean-atmosphere system evolves in response to variations in the total mass of carbon within the capacitor, in this case seafloor methane.

[39] To vary the total mass of seafloor methane, we changed the flux of AOM to achieve reasonable agreement with the  $\delta^{13}\text{C}$  of bulk sediment (Figures 6 and 7). This AOM forcing is as follows: from 1.0 to  $0.6 \times 10^{12} \text{ mol yr}^{-1}$  over the first 4 Myr (62 to 58 Ma), from 0.6 to  $1.5 \times 10^{12} \text{ mol yr}^{-1}$  over the next 5 Myr (58 to 53 Ma), from  $1.5 \times 10^{12} \text{ mol yr}^{-1}$  to  $1.0 \times 10^{12} \text{ mol yr}^{-1}$  over 2.5 Myr (53 to 50.5 Ma), and constant at  $1.0 \times 10^{12} \text{ mol yr}^{-1}$  until 48 Ma (Figures 6a and 7a). The underlying rationale for this approach is that the long-term flux of carbon through AOM should relate to the mass of gas hydrate in marine sediment, which should be dictated mainly by deep ocean temperature [Dickens, 2001a, 2001b, 2003]. It also should be stressed that these AOM fluxes are not hugely different than those ( $\sim 0.6 \times 10^{12} \text{ mol yr}^{-1}$ ) assumed in previous modeling exercises devoted to understanding the short-term negative  $\delta^{13}\text{C}$  excursion across the PETM

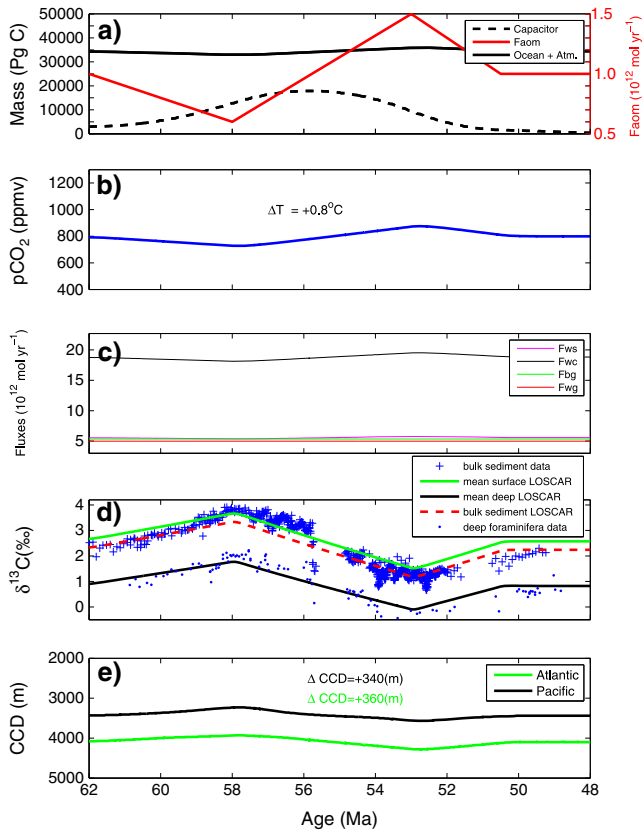


**Figure 7.** Same as Figure 6, except DIC:TA input from AOM = 1:1.

[Dickens, 2003]. The weathering feedback used here is weaker compared to that in standard GEOCARB modeling, but the same as that used in Simulation 2.

[40] We considered two cases for simulation, one in which carbon exchange from seafloor methane to the ocean occurs as  $\text{CO}_2$  (Simulation 3) and one in which such exchange occurs as  $\text{HCO}_3^-$  (Simulation 4). The reason for this is that dissolved inorganic carbon (DIC) can escape seafloor gas hydrate systems as  $\text{CO}_2$  (through aerobic oxidation of  $\text{CH}_4$  in the water column) or as  $\text{HCO}_3^-$  (through  $\text{CH}_4$  generation in sediment, through anaerobic oxidation of  $\text{CH}_4$  in sediment, and subsequent diffusion of both) [Dickens, 2003, 2011]; however, these outputs of DIC should have different total alkalinity (TA). For  $\text{CO}_2$ , the DIC to TA ratio is 1:0; for  $\text{HCO}_3^-$ , the DIC to TA ratio is 1:1.

[41] According to our simulations (Figures 6 and 7), the capacitor grows from an initial mass  $0.25 \times 10^{18}$  mol C (3000 Pg C) at 62 Ma to a peak mass of about  $1.49 \times 10^{18}$  mol C ( $\sim 17,900$  Pg C) around 55.8 Ma, or just before the PETM (55.53 Ma on the timescale of the bulk  $\delta^{13}\text{C}$  record used for modeling). From then, the capacitor steadily discharges, until it is almost completely empty by 50 Ma. Note that the peak mass occurs about 2.5 Myr after the peak in surface water  $\delta^{13}\text{C}$ . This is because the flux of carbon through AOM is decreasing but still above that of quasi steady state conditions. Should the long-term drop in  $\delta^{13}\text{C}$  across the LPEE relate to diminishing fluxes from a large and dynamic gas hydrate capacitor, one that grew through the middle to late Paleocene, the PETM necessarily had to occur at about the time of maximum seafloor methane mass.

[42] The capacitor simulations also give intriguing results regarding the  $\delta^{13}\text{C}$  gradient and the CCD deepening during the LPEE (Figures 6 and 7). Namely, the  $\delta^{13}\text{C}$  gradient and the CCD deepening produced in the capacitor simulations are more consistent with the observations (Figures 6e and 7e), which is due to smaller carbon fluxes (explained below). Comparison of the capacitor simulations (Simulations 3 and 4) shows that the increased alkalinity scenario damps the CCD and  $p\text{CO}_2$  variations. This is due to an increased buffer capacity of the ocean as a consequence of the higher alkalinity.

[43] At this point, a methane hydrate capacitor seems a plausible cause for both the short-term and the long-term carbon cycle trends across the LPEE. However, for this explanation to be fully compatible with observations, it requires different perspectives on Earth system sensitivity and gas hydrate masses.

[44] Because  $\text{CH}_4$  in gas hydrate is typically very depleted in  $^{13}\text{C}$  (probably  $\delta^{13}\text{C} < 70\text{‰}$  in the early Paleogene) [Dickens, 2003], the amounts and fluxes of carbon necessary to drive the observed  $\delta^{13}\text{C}$  trends are much smaller than those required by burial of organic carbon. This is reflected by the predicted modest temperature rise ( $0.8$  to  $1.6^\circ\text{C}$ ) between 58 and 52 Ma (Figures 6 and 7), assuming an Earth system sensitivity of  $3^\circ\text{C}$  per doubling of  $p\text{CO}_2$ . Either Earth system sensitivity has to be more than twice the canonical value of  $3^\circ\text{C}$ , or a good fraction of the warming during the LPEE (as well as the preceding cooling) was unrelated to changes in carbon cycling represented by  $\delta^{13}\text{C}$  and CCD records. We note the latter is consistent with the temporal lag between  $\delta^{18}\text{O}$  and  $\delta^{13}\text{C}$  (Figure 1b), as well as an explanation involving gas hydrates, because changes in carbon fluxes would result from warming (and cooling) rather than the other way around [Dickens *et al.*, 1997; Dickens, 2011]. This same issue—Earth surface warming leading massive carbon addition—has been emphasized in papers regarding the short-term hyperthermal events of the early Paleogene [e.g., Sluijs *et al.*, 2012; Zeebe *et al.*, 2009].

[45] The global mass of gas hydrates in marine sediment and the rates to and from this reservoir remain uncertain for any time in Earth's history, including the present day. Various studies have suggested that gas hydrates on modern continental slopes store between 1000 and 22,000 Pg C [Kvenvolden, 1993; Dickens, 2001b; Milkov, 2004; Archer, 2007; Burwicz *et al.*, 2010]. As pointed out by Dickens [2011], the lower estimates do not conform to basic field data, and we accept 5000–10,000 Pg C as reasonable for the present day. In our model simulations, the masses of the gas hydrate capacitor at initial steady state conditions (62 Ma) are smaller than this value. However, during the late Paleocene, the mass grows much larger. Benthic foraminifera  $\delta^{18}\text{O}$  records suggest an  $\sim 4$  Myr interval of bottom water cooling that preceded the LPEE (Figure 1a). In theory, this  $3\text{--}4^\circ$  cooling would nearly double the volume of the methane capacitor by thickening the gas hydrate stability zone in marine sediment [Dickens, 2001a, 2001b]. The fraction of organic carbon entering sediment and forming methane in the past also may have been significantly greater than today because of lower dissolved  $\text{O}_2$ , lower dissolved  $\text{SO}_4^{2-}$ , and faster methanogenesis [Gu *et al.*, 2011; Dickens, 2011]. Is it possible that these factors created conditions that would allow a methane hydrate capacitor to grow

sufficiently large such that its collapse drove the carbon cycle changes during the LPEE? We acknowledge that a peak mass of  $\sim 18,000$  Pg C, as required in our simulations, does seem high for Paleocene conditions.

[46] Other organic carbon capacitors can be suggested and simulated with a coupled LOSCAR-GEOCARB model, notably peat or permafrost carbon [Kurtz *et al.*, 2003]. However, we emphasize that such modeling will lead to basic issues concerning the mass balance and the CCD. The  $\delta^{13}\text{C}$  of terrestrial carbon in the early Paleogene was nominally  $-30\text{‰}$  [Jaramillo *et al.*, 2010; Samanta *et al.*, 2013]. Consequently, relative to methane, a much greater mass of carbon is required to drive the long-term changes in  $\delta^{13}\text{C}$ . For example, initial modeling by Kurtz *et al.* [2003] led to a buildup of 60,000 Pg C in terrestrial carbon pools during the latest Paleocene, compared to the  $\sim 1000$  Pg C in peat [Page *et al.*, 2011] or  $\sim 1600$  Pg C in Arctic permafrost [Tarnocai *et al.*, 2009] at present day. The oxidation of this peat would also cause drops in the CCD more than observed (Figures 5 and 6).

#### 4. Conclusions and Outlook

[47] An interval of the early Paleogene (62 to 48 Ma) was characterized by major perturbations in the global carbon cycle. These include both long-term ( $>1$  Myr) and short-term ( $<200$  kyr) variations in the  $\delta^{13}\text{C}$  of carbon-bearing phases as well as variations in the CCD [e.g., Leon-Rodriguez and Dickens, 2010; McInerney and Wing, 2011; Westerhold *et al.*, 2011; Pälike *et al.*, 2012]. Carbon cycle changes across the hyperthermals have received considerable attention [e.g., Lourens *et al.*, 2005; Stap *et al.*, 2009; Zachos *et al.*, 2010; McInerney and Wing, 2011; Westerhold *et al.*, 2011], while those across the broader time frame (i.e., the background variations) largely have been ignored. Notably, this includes the LPEE (58–52 Ma), when  $\delta^{13}\text{C}$  of marine carbonate decreased by 1.5–2.5‰, and the CCD deepened by several hundreds of meters.

[48] The present study shows that long-term changes in carbon cycling during the LPEE were likely due to a net decrease in organic matter burial. An increase in volcanic degassing seems highly unlikely as the primary cause, although it might have contributed to some degree. This conclusion is based upon a coupled GEOCARB-LOSCAR model and is consistent with previous modeling studies [Kurtz *et al.*, 2003; Hilting *et al.*, 2008]. However, this is the first study to also consider the evolution of the CCD, as well as complete ocean carbonate chemistry, and prognostic surface to deep  $\delta^{13}\text{C}$  gradients. We show that these are essential additional components for constraining possible causes for carbon cycle changes during the studied period.

[49] A fundamental concept to recognize is that a decrease in net organic carbon burial leads to multiple possibilities, especially including increased fluxes from an organic matter reservoir. Given previous work, the two obvious cases are greater oxidation of terrestrial organic matter [Kurtz *et al.*, 2003], and greater fluxes of  $\text{CH}_4$  from the seafloor, which would have been rapidly oxidized in the ocean or atmosphere [Dickens, 2003]. In theory, these different causes for the drop in  $\delta^{13}\text{C}$  across the LPEE can be distinguished from the record of carbonate accumulation on the seafloor (Figures 4–7). This is because the  $\delta^{13}\text{C}$  of terrestrial organic carbon ( $\sim -30\text{‰}$ ) is very different than that of methane in

marine sediment ( $\sim -70\text{‰}$ ), so that changes in  $\delta^{13}\text{C}$  of the exogenic carbon cycle would relate to much different fluxes of carbon.

[50] Unfortunately, the position of the CCD across the Paleocene and early Eocene remains somewhat unconstrained. Between 58 and 52 Ma, it most probably did not deepen by more than 500 to 1000 m [Van Andel, 1975; Hancock *et al.*, 2007; Leon-Rodriguez and Dickens, 2010]. This almost assuredly excludes mantle carbon inputs as a primary cause for prominent carbon cycle changes during the LPEE but leaves discussions on plausible organic carbon sources open to debate. Future modeling studies regarding early Paleogene carbon cycling would greatly benefit from an increased number and spread of early Paleogene CCD records.

[51] Despite the limited CCD records for the LPEE, the modeling used in this study leads to simulations that reproduce observed long-term trends in temperature, carbonate  $\delta^{13}\text{C}$ , and the CCD. The problem is that our modeling is unable to reproduce all these trends quantitatively and collectively. The surface to deep ocean gradient in  $\delta^{13}\text{C}$  can only be reproduced if bulk carbonate records rather than mixed layer planktonic foraminifera records are assumed to reflect surface water changes in  $\delta^{13}\text{C}$ . The predicted temperature rise resulting from carbon cycle changes is much lower than the temperature rise reconstructed from proxies. To some degree, we are not surprised, these same issues have arisen in modeling studies of the short-term hyperthermal events [Zeebe *et al.*, 2009]. Clearly, there are still one or more data-model problems confronting a full understanding of early Paleogene carbon cycle and climate variance.

[52] **Acknowledgments.** We thank Gregory Ravizza, Fred Mackenzie, Lee Kump, and one anonymous reviewer for their time and constructive comments which improved the paper. We are also grateful to Robert Berner for sharing data and model parameters.

#### References

- Archer, D. (2007), Methane hydrate stability and anthropogenic climate change, *Biogeosciences*, 4, 521–544, doi:10.5194/bg-4-521-2007.
- Bemis, B. E., H. J. Spero, J. Bijma, and D. W. Lea (1998), Reevaluation of the oxygen isotopic composition of planktonic foraminifera: Experimental results and revised paleotemperature equations, *Paleoceanography*, 13, 150–160.
- Berner, R. A. (1987), Models for carbon and sulfur cycles and atmospheric oxygen: Application to Paleozoic history, *Am. J. Sci.*, 287, 177–196.
- Berner, R. A. (1990), Atmospheric carbon dioxide over Phanerozoic time, *Science*, 249, 1382–1386.
- Berner, R. A. (1999), A new look at the long-term carbon cycle, *GSA Today*, 9, 1–6.
- Berner, R. A., and D. E. Canfield (1989), A new model of atmospheric oxygen over Phanerozoic time, *Am. J. Sci.*, 289, 331–361.
- Berner, R. A., and Z. Kothavala (2001), GEOCARB III: A revised model of atmospheric  $\text{CO}_2$  over Phanerozoic time, *Am. J. Sci.*, 304, 397–437.
- Berner, R. A., A. C. Lasaga, and R. M. Garrels (1983), The carbonate-silicate geochemical cycle and its effect in atmospheric carbon dioxide over the past 100 million years, *Am. J. Sci.*, 283, 641–683.
- Bice, K. L., and J. Marotzke (2002), Could changing ocean circulation have destabilized methane hydrate at the Paleocene/Eocene boundary?, *Paleoceanography*, 17, 1018, doi:10.1029/2001PA000678.
- Bijl, P. K., S. Schouten, A. Sluijs, G. J. Reichert, J. C. Zachos, and H. Brinkhuis (2009), Early Palaeogene temperature evolution of the southwest Pacific Ocean, *Nature*, 461, 776–779, doi:10.1038/nature08399.
- Birch, H. S., H. K. Coxall, and P. N. Pearson (2012), Evolutionary ecology of Early Paleocene planktonic foraminifera: Size, depth habitat and symbiosis, *Paleobiology*, 38(3), 374–390.
- Brady, P. V., R. I. Dorn, A. J. Brazel, J. Clark, R. B. Moore, and T. Glidewell (1999), Direct measurement of the combined effects of lichen, rainfall, and temperature on silicate weathering, *Geochim. Cosmochim. Acta*, 63, 3293–3300.

- Burwicz, E. B., L. H. Rüpke, and K. Wallmann (2010), Estimation of the global amount of submarine gas hydrates formed via microbial methane formation based on numerical reaction-transport modeling and a novel parameterization of Holocene sedimentation, *Geochimica et Cosmochimica Acta*, **75**, 4562–4576.
- Cramer, B. S., J. R. Toggweiler, J. D. Wright, M. E. Katz, and K. G. Miller (2009), Ocean overturning since the Late Cretaceous: Inferences from a new benthic foraminiferal isotope compilation, *Paleoceanography*, **24**, PA4216, doi:10.1029/2008PA001683.
- D'Hondt, S., J. C. Zachos, and G. Schultz (1994), Stable isotopic signals and photosymbiosis in late Paleocene planktic foraminifera, *Paleobiology*, **20**, 391–406.
- Dickens, G. R. (2001a), "Carbon addition and removal during the late Paleocene thermal maximum: Basic theory with a preliminary treatment of the isotope record at Ocean Drilling Program Site 1051, Blake Nose." Western North Atlantic Paleogene and Cretaceous Paleocyanography, in *Western North Atlantic Paleogene and Cretaceous Paleocyanography*, vol. 183, edited by D. Kroon, R. D. Norris, and A. Klaus, pp. 293–306, Geological Society Special Publication, London, doi:10.1144/GSL.SP.2001.183.01.14.
- Dickens, G. R. (2001b), The potential volume of oceanic methane hydrates with variable external conditions, *Org. Geochem.*, **32**, 1132–1193.
- Dickens, G. R. (2003), Rethinking the global carbon cycle with a large, dynamic and microbially mediated gas hydrate capacitor, *Earth Planet. Sci. Lett.*, **213**, 169–183.
- Dickens, G. R. (2011), Down the rabbit hole: Toward appropriate discussion of methane release from gas hydrate systems during the Paleocene-Eocene thermal maximum and other past hyperthermal events, *Clim. Past*, **7**, 831–846.
- Dickens, G. R., and J. Backman (2013), Core alignment and composite depth scale for the lower Paleogene through uppermost Cretaceous interval at Deep Sea Drilling Project Site 577, *Newsl. Stratigr.*, **46**(1), 47–68, doi:10.1127/0078-0421/2013/0027.
- Dickens, G. R., M. M. Castillo, and J. C. G. Walker (1997), A blast of gas in the latest Paleocene: Simulating first-order effects of massive dissociation of oceanic methane hydrate, *Geology*, **25**, 259–262.
- Edgar, K. M., S. M. Bohaty, S. J. Gibbs, P. F. Sexton, R. D. Norris, and P. A. Wilson (2012), Symbiotic "bleaching" in planktic foraminifera during the Middle Eocene Climatic Optimum, *Geology*, **41**, 15–18.
- Erdman, J. G., and K. S. Schorno (1978a), Geochemistry of carbon: Deep Sea Drilling Project leg 38, in *Init. Rep. DSDP*, vol. 38, edited by M. Talwani et al., pp. 791–799, U.S. Govt. Printing Office, WA.
- Erdman, J. G., and K. S. Schorno (1978b), Geochemistry of carbon: Deep Sea Drilling Project leg 40, in *Init. Rep. DSDP*, vol. 40 (Suppl.), edited by H. M. Bolli et al., pp. 651–658, U.S. Govt. Printing Office, WA.
- Erdman, J. G., and K. S. Schorno (1978c), Geochemistry of carbon: Deep Sea Drilling Project leg 40, in *Init. Rep. DSDP*, vol. 41, edited by Y. Lancelot et al., pp. 651–658, U.S. Govt. Printing Office, WA.
- Erdman, J. G., and K. S. Schorno (1979), Geochemistry of carbon: Deep Sea Drilling Project legs 47A and B, in *Init. Rep. DSDP*, vol. 47, Part 2, edited by J.-C. Sibuet et al., pp. 651–658, U.S. Govt. Printing Office, WA.
- Expedition 329 Scientists (2011), Expedition 329 summary. *Proc. Integr. Drill. Program*, **329**, doi:10.2204/iodp.proc.329.101.2011.
- Freeman, K. H., and J. M. Hayes (1992), Fractionation of carbon isotopes by phytoplankton and estimates of ancient CO<sub>2</sub> levels, *Global Biogeochem. Cycles*, **6**(2), 185–198.
- Gislason, S. R., and E. H. Oelkers (2003), Mechanism, rates, and consequences of basaltic glass dissolution: II. An experimental study of the dissolution rates of basaltic glass as a function of pH and temperature, *Geochim. Cosmochim. Acta*, **67**, 3817–3832.
- Gislason, S. R., et al. (2009), Direct evidence of the feedback between climate and weathering, *Earth Planet. Sci. Lett.*, **277**, 213–222.
- Gu, G., G. R. Dickens, G. Bhatnagar, F. S. Colwell, G. J. Hirasaki, and W. G. Chapman (2011), Abundant early Palaeogene marine gas hydrates despite warm deep-ocean temperatures, *Nat. Geosci.*, **4**, 848–851.
- Hancock, H. J. L., G. R. Dickens, E. Thomas, and K. L. Blake (2007), Reappraisal of early Paleogene CCD curves: Foraminiferal assemblages and stable carbon isotopes across the carbonate facies of Perth Abyssal Plain, *Int. J. Earth Sci.*, **96**, 925–946, doi:10.1007/s00531-006-0144-0.
- Hag, B. U., J. Hardenbol, and P. R. Vail (1987), Chronology of fluctuating sea levels since the Triassic (250 million years ago to present), *Science*, **235**, 1156–1167.
- Hayes, J. M., H. Strauss, and A. J. Kaufman (1999), The abundance of <sup>13</sup>C in marine organic matter and isotopic fractionation in the global biogeochemical cycle of carbon during the past 800 Ma, *Chem. Geol.*, **161**, 103–125.
- Hilting, A. K., L. R. Kump, and T. J. Bralower (2008), Variations in the oceanic vertical carbon isotope gradient and their implications for the Paleocene-Eocene biological pump, *Paleoceanography*, **23**, PA3222, doi:10.1029/2007PA001458.
- Hollis, C. J., et al. (2012), Early Paleogene temperature history of the Southwest Pacific Ocean: Reconciling proxies and models, *Earth and Planetary Science Letters*, **349–350**, 53–66.
- Horita, J., H. Zimmermann, and H. D. Holland (2002), Chemical evolution of seawater during the Phanerozoic: Implications from the record of marine evaporites, *Geochim. Cosmochim. Acta*, **66**(21), 3733–3756.
- IPCC (2007), Intergovernmental Panel on Climate Change, *Climate Change 2007: The Physical Science Basis*, 996 pp., Cambridge Univ. Press, Cambridge.
- Kump, L. R. (1991), Interpreting carbon-isotope excursions: Strangelove oceans, *Geology*, **19**, 299–302.
- Kump, L. R., and M. A. Arthur (1999), Interpreting carbon-isotope excursions: Carbonates and organic matter, *Chem. Geol.*, **161**, 181–198.
- Kurtz, A., L. R. Kump, M. A. Arthur, J. C. Zachos, and A. Paytan (2003), Early Cenozoic decoupling of the global carbon and sulfur cycles, *Paleoceanography*, **18**, 1090, doi:10.1029/2003PA000908.
- Kvenvolden, K. A. (1993), Gas hydrates: Geological perspective and global change, *Rev. Geophys.*, **31**, 173–187.
- Jaramillo, C., et al. (2010), Effects of rapid global warming at the Paleocene-Eocene, *Science*, **330**, 957–961.
- Lasaga, A. C., R. A. Berner, and R. M. Garrels (1985), An improved geochemical model of atmospheric CO<sub>2</sub> fluctuations over the past 100 million years, in *The Carbon Cycle and Atmospheric CO<sub>2</sub>: Natural Variations Archean to Present Geophys. Monogr. Ser.*, vol. 32, edited by E. T. Sundquist and W. S. Broecker, pp. 397–411, AGU, Washington, D. C., doi:10.1029/GM032p0397.
- Leon-Rodriguez, L., and G. R. Dickens (2010), Constraints on ocean acidification associated with rapid and massive carbon injections: The early Paleogene record at ocean drilling program site 1215, equatorial Pacific Ocean, *Palaeogeogr. Palaeoclimatol.*, **298**, 409–420.
- Lourens, L. J., A. Sluijs, D. Kroon, J. C. Zachos, E. Thomas, U. Röhl, J. Bowles, and I. Raffi (2005), Astronomical pacing of late Palaeocene to early Eocene global warming events, *Nature*, **435**(7045), 1083–1087, doi:10.1038/nature03814.
- Lowenstein, T. K., M. N. Timofeeff, S. T. Brennan, L. A. Hardie, and R. V. Demicco (2001), Oscillation in Phanerozoic seawater chemistry: Evidence from fluid inclusions, *Science*, **294**, 1086–1088.
- Macko, S. A., and C. P. G. Pereira (1990), Neogene paleoclimate development of the Antarctic Weddell Sea region: Organic geochemistry, in *Proc. ODP. Sci. Results*, vol. 113, edited by P. F. Barker et al., Ocean Drilling Program, College Station, TX, pp. 881–897.
- Milkov, A. V. (2004), Global estimates of hydrate-bound gas in marine sediments: How much is really out there?, *Earth-Sci. Rev.*, **66**, 183–197.
- McInerney, F. A., and S. Wing (2011), A perturbation of carbon cycle, climate, and biosphere with implications for the future, *Ann. Rev. Earth Planet. Sci.*, **39**, 489–516.
- Miller, K. G., J. V. Browning, S. F. Pekar, and P. J. Sugarman (1997), Cenozoic evolution of the New Jersey coastal plain: Changes in sea level, tectonics, and sediment supply, *Proc. Ocean Drill. Program, Sci. Results*, **150X**, 361–373.
- Müller, R. D., M. Sdrolias, C. Gaina, B. Steinberg, and C. Hein (2008), Long-term sea-level fluctuations driven by ocean basin dynamics, *Science*, **319**(5868), 1357–1362, doi:10.1126/science.1151540.
- Nicolo, M. J., G. R. Dickens, C. J. Hollis, and J. C. Zachos (2007), Multiple early Eocene hyperthermals: Their sedimentary expression on the New Zealand continental margin and in the deep sea, *Geology*, **35**(8), 699–702, doi:10.1130/G23648A.
- Page, S. E., J. O. Rieley, and C. J. Banks (2011), Global and regional importance of the tropical peatland carbon pool, *Global Change Biol.*, **17**, 798–818.
- Pälike, H., et al. (2012), A Cenozoic record of the equatorial Pacific carbonate compensation depth, *Nature*, **488**, 609–614.
- Park, J., and D. L. Royer (2011), Geologic constraints on the glacial amplification of Phanerozoic climate sensitivity, *Am. J. Sci.*, **311**, 1–26, doi:10.2475/01.2011.01.
- Poore, H. R., R. Samworth, N. J. Jones, White S. M., and I. N. McCave (2006), Neogene overflow of northern component water at the Greenland-Scotland Ridge, *Geoch. Geoph. Geosys.*, **7**, Q06010, doi:10.1029/2005GC001085.
- Reeburgh, W. (1976), S., Methane consumption in Cariaco Trench waters and sediments, *Earth Planet. Sci. Lett.*, **28**, 337–344.
- Ridgwell, A., and R. E. Zeebe (2005), The role of the global carbonate cycle in the regulation and evolution of the Earth system, *Earth Planet. Sci. Lett.*, **234**, 299–315.
- Samanta, A., A. Sarkar, M. K. Bera, J. Rai, and S. S. Rathore (2013), Late Paleocene-early Eocene carbon isotope stratigraphy from a near-terrestrial tropical section and antiquity of Indian mammals, *J. Earth Syst. Sci.*, 1–9.

- Samworth, R., and H. R. Poore (2005), Understanding past ocean circulations: A nonparametric regression case study, *Stat. Modell.*, *5*, 289–307.
- Shackleton, N. J. (1974), Attainment of isotopic equilibrium between ocean water and the benthonic foraminifera genus *Uvigerina*: Isotopic changes in the ocean during the last glacial., *Cent. Nat. Rech., Sci. Colloq. Int.*, *219*, 203–209.
- Shackleton, N. J. (1986), Paleogene stable isotope events, *Palaeogeogr. Palaeoclimatol. Palaeocol.*, *57*, 91–102.
- Shackleton, N. J., M. A. Hall, and A. Boersma (1984), Oxygen and carbon isotope data from Leg 74 foraminifers, *Initial Rep. Deep Sea Drill. Proj.*, *74*, 599–612.
- Sluijs, A., and G. D. Dickens (2012), Assessing offsets between the  $\delta^{13}\text{C}$  of sedimentary components and the global exogenic carbon pool across early Paleogene carbon cycle perturbations, *Global Biogeochem. Cycles*, *26*, GB4005, doi:10.1029/2011GB004224.
- Sluijs, A., H. Brinkhuis, S. Schouten, S. M. Bohaty, C. M. John, J. C. Zachos, G. J. Reichert, J. S. Sinninghe Damste, E. M. Crouch, and G. R. Dickens (2012), Environmental precursors to light carbon input at the Paleocene/Eocene boundary, *Nature*, *450*(7173), 1218–1221, doi:10.1038/nature06400.
- Stap, L., A. Sluijs, E. Thomas, and L. J. Lourens (2009), Patterns and magnitude of deep sea carbonate dissolution during Eocene thermal maximum 2 and H2, Walvis Ridge, southeastern Atlantic Ocean, *Paleoceanography*, *24*, PA1211, doi:10.1029/2008PA001655.
- Stein, R., B. Boucsein, and H. Meyer (2006), Anoxia and high primary production in the Paleogene central Arctic Ocean: First detailed records from Lomonosov Ridge, *Geophys. Res. Lett.*, *33*, L18606, doi:10.1029/2006GL026776.
- Tarnocai, C., J. G. Canadell, E. A. G. Schuur, P. Kuhry, G. Mazhitova, and S. Zimov (2009), Soil organic carbon pools in the northern circumpolar permafrost region, *Global Biogeochem. Cycles*, *23*, PA1211, doi:10.1029/2008GB003327.
- Tyrrell, T., and R. E. Zeebe (2004), History of carbonate ion concentration over the last 100 million years, *Geochim. Cosmochim. Acta*, *68*(17), 3521–3530.
- Van Andel, T. (1975), Mesozoic/Cenozoic calcite compensation depth and the global distribution of calcareous sediments, *Earth Planet. Sci. Lett.*, *26*, 187–194.
- Veizer, J., et al. (1999),  $^{87}\text{Sr}/^{86}\text{Sr}$ ,  $\delta^{13}\text{C}$  and  $\delta^{18}\text{O}$  evolution of Phanerozoic seawater, *Chem. Geol.*, *161*, 59–88.
- Westerhold, T., U. Röhl, I. Raffi, E. Fornacian, S. Monechi, V. Reale, J. Bowles, and H. F. Evans (2008), Astronomical calibration of the Paleocene time, *Palaeogeogr. Palaeoclimatol. Palaeocol.*, *257*, 377–403.
- Westerhold, T., U. Röhl, B. Donner, H. K. McCarren, and J. C. Zachos (2011), A complete high-resolution Paleocene benthic stable isotope record for the central Pacific (ODP Site 1209), *Paleoceanography*, *26*, PA2216, doi:10.1029/2010PA002092.
- Zachos, J. C., H. McCarren, B. Murphy, U. Röhl, and T. Westerhold (2010), Tempo and scale of late Paleocene and Early Eocene carbon isotope cycles: Implications for the origin of hyperthermals, *Earth Planet. Sci. Lett.*, *299*, 242–249.
- Zachos, J. C., M. Pagani, L. Sloan, E. Thomas, and K. Billups (2001), Trends, rhythms, and aberrations in global climate 65 Ma to present, *Science*, *292*, 686–693.
- Zeebe, R. E. (2012), LOSCAR: Long-Term Ocean-Atmosphere-Sediment Carbon Cycle Reservoir Model v2.0.4, *Geosci. Model Dev.*, *1*, 149–166.
- Zeebe, R. E., and P. Westbroek (2003), A simple model for the  $\text{CaCO}_3$  saturation state of the ocean: The “Strangelove,” the “Neritan,” and the “Cretan” Ocean, *Geochem. Geophys. Geosyst.*, *4*(12), 1104, doi:10.1029/2003GC000538.
- Zeebe, R. E., and D. A. Wolf-Gladrow (2001), *CO<sub>2</sub> in Seawater: Equilibrium, Kinetics, Isotopes*, pp. 346, Elsevier Oceanography Series, Amsterdam.
- Zeebe, R. E., J. C. Zachos, and G. R. Dickens (2009), Carbon dioxide forcing alone insufficient to explain Palaeocene-Eocene Thermal Maximum warming, *Nat. Geosci.*, *2*, 576–580, doi:10.1038/NGEO578.
- Zhou, L., and F. T. Kyte (1992), Sedimentation history of the south Pacific pelagic clay province over the last 85 million years inferred from the geochemistry of Deep Sea Drilling Project Hole 596, *Paleoceanography*, *7*, 441–465.